AI-Assisted Physical Modeling of Sun Glint to Improve Inter-Sensor Consistency of Remote Sensing Reflectance in Coastal Waters

Milad Niroumand-Jadidi [1], Lorenzo Mentaschi [2], Sonia Silvestri [3]

[1] Interdepartmental Research Center for Environmental Sciences; University of Bologna, Ravenna, Italy – milad.niroumand@unibo.it
[2] Department of Physics and Astronomy (DIFA), University of Bologna, Bologna, Italy - lorenzo.mentaschi@unibo.it
[3] Department of Biological, Geological, and Environmental Sciences, University of Bologna, Bologna, Italy – sonia.silvestri5@unibo.it

Keywords: Sun Glint, Coastal Waters, Machine Learning, Physical Modeling, WASI-AI, Sensor Harmonization.

Abstract

The remote sensing of biophysical parameters in aquatic systems, such as water constituents, depends strongly on the quality of the spectral data. Sun glint, specular reflection from the water surface, is a major artifact that can substantially contaminate the remote sensing reflectance (R_{rs}). Accurate modeling of sun glint is therefore essential, particularly in multi-sensor analyses, to ensure seamless R_{rs} and water constituent products. Here, we build upon the recently developed WASI-AI model to mitigate sun-glint effects. WASI-AI is an AI-assisted physical inversion that offers key advantages over traditional physics-only approaches, including improved handling of spectral ambiguities and significantly faster inversions. We evaluate the effectiveness of WASI-AI's glint correction capability through an inter-sensor consistency analysis between Landsat-9 and Sentinel-2. The analysis uses near-simultaneous acquisitions over optically complex coastal waters of the Adriatic Sea. The two overpasses are only a few minutes apart, which allows us to assume stable bio-optical conditions. In contrast, sun glint can vary rapidly because it is sensitive to viewing and illumination geometry as well as wind-driven surface roughness and currents. These factors may affect the data from the two sensors differently, even within a short time window. Our results show that the WASI-AI glint correction identifies substantial differences in both the magnitude and spatial patterns of sun glint between the near-simultaneous Landsat-9 and Sentinel-2 acquisitions. The R_{rs} consistency analysis demonstrates that, after glint correction, agreement between corresponding bands of the two sensors improves on average by 6% in R^2 and by 5% in normalized root-mean-square difference.

1. Introduction

The growing availability of diverse satellite missions has significantly expanded the capacity to monitor aquatic systems (Ngamile et al., 2025; Niroumand-Jadidi et al., 2025). In particular, the study of optically complex inland and coastal waters has benefited from high-spatial-resolution sensors such as Landsat-8/9 and Sentinel-2 (Dörnhöfer et al., 2016; Khan et al., 2024; Niroumand-Jadidi et al., 2022; Zaghian et al., 2023). However, differences in radiometric, spectral, and spatial characteristics among these sensors inevitably introduce inconsistencies in the derived products, complicating multi-sensor analyses (Hafeez et al., 2022). Therefore, improving the consistency of data and products derived from multi-sensor analyses is essential. Combining observations from multiple satellites enhances the temporal resolution, which is necessary for capturing the dynamics of biophysical parameters such as water constituents. For instance, this enhanced temporal coverage can support the development of early warning systems for detecting harmful algal blooms (Lin et al., 2021; Niroumand-Jadidi & Bovolo, 2021, 2023).

Optical remote sensing of water quality and benthic parameters presents significant challenges due to the inherently low signal-to-noise ratio captured by satellite sensors (Toming et al., 2016). This limitation stems from the high absorption of downwelling irradiance by water bodies. Consequently, the observed satellite signal is highly susceptible to contamination from atmospheric interference and sun glint (Gordon, 1997). The remote sensing reflectance (R_{rs}), defined as the ratio of water-leaving radiance to downwelling irradiance just above the water surface (Mobley, 1999), represents a fundamental product in aquatic remote sensing, as it underpins the retrieval of water-column constituents and, in optically shallow areas, benthic properties. Accurate estimation of R_{rs} requires robust atmospheric correction and careful modeling of surface-related noise sources, particularly sun-glint.

Sun glint, caused by specular reflections of sunlight on the water surface, can be comparable or even much larger than the intensity of the water-leaving signal, complicating accurate retrieval of biophysical parameters (Gege & Groetsch, 2016; Kay et al., 2009). Notably, even when the sensor avoids direct alignment with the sun's specular reflection, surface roughness, induced by ripples and waves, can redirect sunlight toward the sensor (Gege & Groetsch, 2016). Thus, sun glint correction is a critical step in processing multi-sensor temporal satellite imagery to ensure seamless R_{rs} products, which are essential for generating consistent estimates of water quality and benthic parameters.

Various methods have been developed to mitigate the sun glint effect in inland and coastal waters, most of which rely on the assumption that water-leaving radiance is negligible in the near-infrared (NIR) region of the spectrum. Consequently, any residual NIR radiance following atmospheric correction is typically attributed to sun glint (Hochberg et al., 2003; Kay et al., 2009). In these methods, a representative deep-water spectrum is analyzed to determine the relationship between NIR radiance and the corresponding glint contribution. However, these approaches become less reliable when the NIR signal is non-negligible, particularly in optically complex and highly turbid inland and nearshore coastal waters. The use of NIR-based glint correction techniques can lead to overcorrection in turbid waters, where the water-leaving signal in the NIR region is not negligible. Alternative approaches have therefore been developed for waters with significant NIR reflectance. For example, one method exploits the presence and depth of the oxygen absorption feature near 760 nm, which is primarily applicable to hyperspectral sensors that include this spectral band (Kutser et al., 2009). For turbid waters, some approaches estimate sun glint contributions using shortwave-infrared (SWIR) wavelengths and then extrapolate these estimates toward the near-infrared and visible bands (Harmel et al., 2018; Vanhellemont, 2019). However, despite these developments, accurately modeling sun glint in such conditions still requires further investigation.

In this study, we build upon a recently developed model, WASI-AI (Niroumand-Jadidi & Gege, 2025), which integrates artificial intelligence (AI) with physical modeling to enhance the retrieval of biophysical parameters (water constituents and benthic parameters in shallow waters) while effectively mitigating sun-glint artifacts. We adapt the WASI-AI model to process Landsat-9 and Sentinel-2 imagery acquired near-simultaneously in coastal waters, and we evaluate the effectiveness of sun glint mitigation by analyzing the inter-sensor consistency of R_{rs} before and after correction. Although Landsat-9 and Sentinel-2 share similarities in the design of some spectral bands, they still differ in their spectral, radiometric, and spatial resolutions. These differences influence the sensors’ sensitivity to sun-glint effects. Even when images are acquired only minutes apart, and the water constituents can be assumed stable, the magnitude of sun glint may vary substantially. This variability arises from rapid changes in water-surface roughness driven by wind and tidal dynamics, as well as differences in the illumination and viewing geometry of the two sensors. Consequently, near-simultaneous Landsat-9 and Sentinel-2 acquisitions provide an effective testbed for evaluating the performance of the WASI-AI model in sun-glint modeling and for assessing its ability to produce consistent R_{rs} products, given that sun glint represents a major variable component influencing R_{rs}.

In the next section, we describe the WASI-AI model, including the implemented sun-glint correction method. Section 3 introduces the study area and the satellite imagery dataset. Section 4 presents the results together with the discussion, followed by the concluding remarks in Section 5.

2. Methods

WASI-AI is a newly developed model implemented within the publicly available Water Color Simulator (WASI) software (Niroumand-Jadidi & Gege, 2025). It integrates AI into physics-based spectrum-matching inversion, offering significant benefits while retaining the core strengths of physical modeling, such as adaptability to diverse bio-optical conditions and sensor independence. The key advancements of WASI-AI include its ability to resolve spectral ambiguity and perform inversions at substantially higher speeds than traditional physics-based approaches. WASI-AI first performs physical inversion on a small subset (a few hundred) of image pixels. The physical inversion model is called WASI-2D that incorporates well-established optically shallow or deep water physical equations through an iterative spectrum matching inversion procedure (Gege, 2014). The inverted samples are then divided into training and validation sets. The training samples are subsequently employed to train neural networks, which are then applied to retrieve the parameters of interest, including sun glint, across the entire image. The validation samples are used to assess the consistency between the retrievals of the AI-assisted physical model (WASI-AI) and the fully physics-based model (WASI-2D). A weak agreement between WASI-AI and WASI-2D for a given parameter indicates that the inversion is affected by spectral ambiguity, signaling the need to adjust the parameterization of the physical model. In the physical component of WASI-AI, the user must specify which parameters are retrieved (fit parameters) and which are held constant across the image. To reduce spectral ambiguity and increase the degrees of freedom available to the physical model, the number of fit parameters should be minimized as much as possible (Niroumand-Jadidi et al., 2020, 2021). A schematic representation of the model is shown in Figure 1, and a detailed description of the WASI-AI framework is provided in (Niroumand-Jadidi & Gege, 2025).

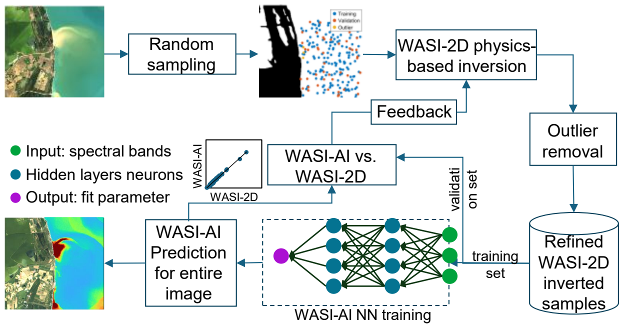

Figure 1. Schematic overview of the WASI-AI framework, illustrating the AI-assisted physical inversion process for retrieving fit parameters such as sun glint. Adapted from (Niroumand-Jadidi & Gege, 2025).

.

The physical modeling of sun glint follows the analytic framework proposed by (Gege & Groetsch, 2016), which formulates the intensity and spectral dependence of sun and sky glint. Central to this formulation is the g_{dd} (sr^{-1}) parameter, representing the fraction of sky radiance due to direct solar radiation (sun glint). Within WASI-AI, this model serves as the foundation for estimating glint contributions and subsequently correcting the R_{rs} data.

The water-surface reflections are simulated with the three-component model proposed by Gege (2014), which quantifies the contributions of different sky-radiance components reflected in the sensor’s viewing direction.

$$L_{sky}(\lambda) = g_{dd}E_{dd}(\lambda) + g_{dsr}E_{dsr}(\lambda) + g_{dsa}E_{dsa}(\lambda), \quad (1)$$

where $E_{dd}(\lambda)$ = direct downwelling irradiance from the sun disk
$E_{dsr}(\lambda)$= diffuse downwelling irradiance caused by Rayleigh scattering
$E_{dsa}(\lambda)$ = diffuse downwelling irradiance caused by aerosol scattering
g_{dd}, g_{dsr} and g_{dsa} = weighting factors of each of above radiance components

The three radiance components in Equation (1) represent the contribution of sun-glint and the portions of skylight, both its blue and gray components, reflected by molecules and atmospheric aerosols. These components, $E_{dd}(\lambda)$, $E_{dsr}(\lambda)$ and $E_{dsa}(\lambda)$, are parameterized as functions of aerosols, water vapor, and ozone according to (Gege, 2012), which is based on the model originally proposed by (Gregg & Carder, 1990). The factors g_{dd}, g_{dsr}, and g_{dsa} specify the proportion of each irradiance component reflected in the sensor’s direction. Variations in surface roughness, such as wave motion, cause these factors to differ from one pixel to another. An idealized isotropic sky is characterized by assigning equal fractions of sky radiance to molecular and aerosol scattering, with $g_{dsr} = g_{dsa} = 1/\pi$. The surface reflectance $R_{rs}^{surf}(\lambda)$ can be formulated as:

$$R_{rs}^{surf}(\lambda) = \rho_L(\theta_v) \times \frac{L_{sky}(\lambda)}{E_{dd}(\lambda)+E_{dsr}(\lambda)+E_{dsa}(\lambda)}, \tag{2}$$

where $\rho_L(\theta_v)$ = Fresnel reflection for a viewing angle of θ_v (Jerlov, 1976). $\rho_L(0) = 0.020$ for nadir observation.

The surface reflection model (Equation 2) is applied within the physical component of the WASI-AI model, i.e., WASI-2D, to correct the surface reflections, where any of g_{dd}, g_{dsr} or g_{dsa} may be assumed as fit parameters. Because the spectral signature of sun glint resembles that of atmospheric straylight, the parameter g_{dd} can also partially compensate for atmospheric-correction errors arising from under- or overestimation of the path radiance (Gege & Groetsch, 2016).

WASI-AI relies on atmospherically corrected imagery because its physical module (WASI-2D) does not include an atmospheric radiative transfer component. In this study, we employ ACOLITE atmospheric correction (Vanhellemont, 2019; Vanhellemont & Ruddick, 2018) to derive the R_{rs} without a glint correction. In this context, given the strong influence of sun glint on aquatic parameter retrieval and the presence of residual atmospheric artifacts even after correction, g_{dd} typically needs to be treated as a fit parameter when processing most images (Niroumand-Jadidi et al., 2021). In this study, we treat g_{dd} as a fit parameter to quantify the magnitude of sun-glint contamination, after which the surface-reflected component, $R_{rs}^{surf}(\lambda)$, is subtracted from the ACOLITE R_{rs} (without glint correction) to obtain the glint-corrected R_{rs}. In addition to g_{dd}, chlorophyll-a (Chl-a) and total suspended matter (TSM) are also treated as fit parameters, and each Landsat–Sentinel image pair is subsequently analyzed with WASI-AI using the same parameterization.

Inter-sensor consistency of R_{rs} before and after glint correction is quantified using the coefficient of determination (R^2) and the normalized root-mean-square difference (NRMSD), based on a pixel-by-pixel comparison between Landsat-9 and Sentinel-2 for each spectral band. The RMSD is normalized by the range of R_{rs} values within the corresponding band and expressed as a percentage. To enable pixel-level comparison, both Landsat-9 and Sentinel-2 data are resampled to a 60 m spatial resolution by averaging the pixels. Note that five Landsat-9 bands and their corresponding Sentinel-2 bands in the visible–near-infrared region are used for the R_{rs} comparison.

3. Case Study and Dataset

The case study is located in the north-western Adriatic Sea, along the coastal waters of Emilia–Romagna in Italy. This area represents optically complex waters strongly influenced by the Po River outflow. We selected two pairs of near-simultaneous images from Landsat-9 and Sentinel-2 to investigate the inter-sensor consistency of R_{rs} products before and after sun glint correction. The Landsat-9 and Sentinel scenes were acquired only 26 minutes apart. This short temporal separation ensures that the water’s bio-optical properties remain effectively unchanged, so variations in reflectance between the two images are dominated by differences in sun glint intensity rather than changes in constituent concentrations.

The images selected from August 2023 (Figure 2a) and November 2023 (Figure 2b) exhibit pronounced differences in bio-optical conditions. The November scene contains a substantial sediment load delivered by the river, resulting in much brighter waters due to strong scattering by suspended particles. This contrast provides a suitable dataset for evaluating the performance of the WASI-AI glint correction approach under varying optical regimes. Visual inspection of each Landsat–Sentinel pair acquired on the same date shows broadly consistent water-color patterns after ACOLITE atmospheric correction (Figure 2). However, sun-glint effects are not always visually apparent, making it valuable to also assess inter-sensor differences in glint intensity even when they are not obvious to the eye.

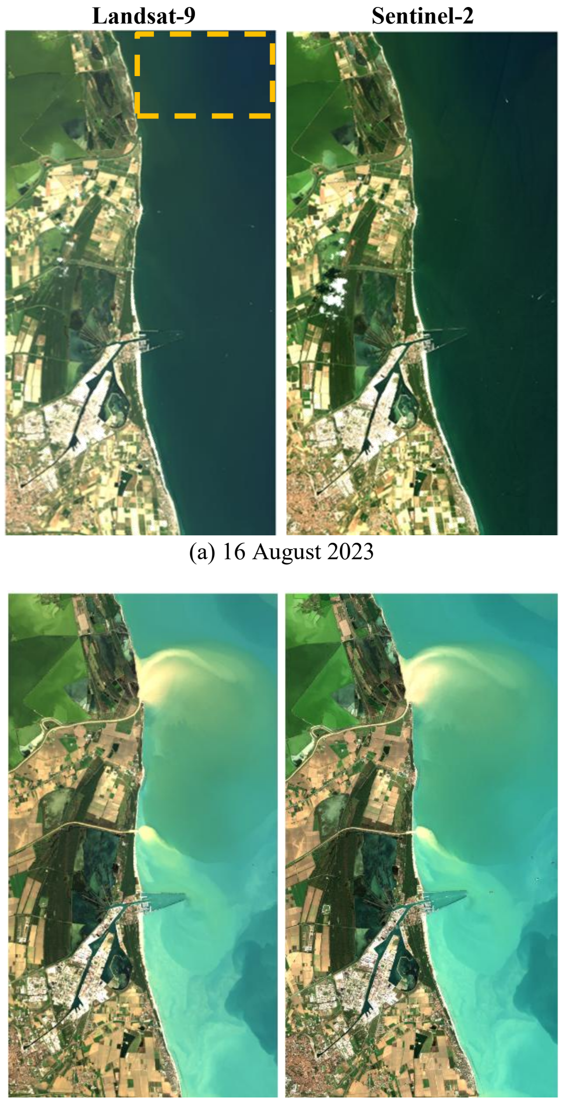

(a) 16 August 2023

(b) 4 November 2023

Figure 2. True-color composite images acquired near-simultaneously by the Landsat-9 and Sentinel-2 sensors, processed using the ACOLITE atmospheric correction. The highlighted box on the Landsat-9 image from August indicates the area used to compare spectral signatures before and after glint correction.

4. Results

Figure 3 presents the glint correction parameter (g_{dd}) for the two pairs of near-simultaneous Landsat-9 and Sentinel-2 images. Notably, the magnitude and spatial pattern of sun glint differ substantially between the two sensors, even though the acquisitions occurred only minutes apart. This underscores the critical importance of applying appropriate glint correction in multi-sensor image analyses to derive consistent R_{rs} and water quality products.

We assessed the consistency of R_{rs} across comparable bands of near-simultaneous Landsat-9 and Sentinel-2 images, both before and after glint correction with WASI-AI, through pixel-by-pixel comparisons at a spatial resolution of 60 m (Table 1). The consistency analysis for both pair of images shows that inter-sensor agreement of R_{rs} bands improves on average by 6% in terms of R^2 and by 5% in terms of NRMSD following the glint correction.

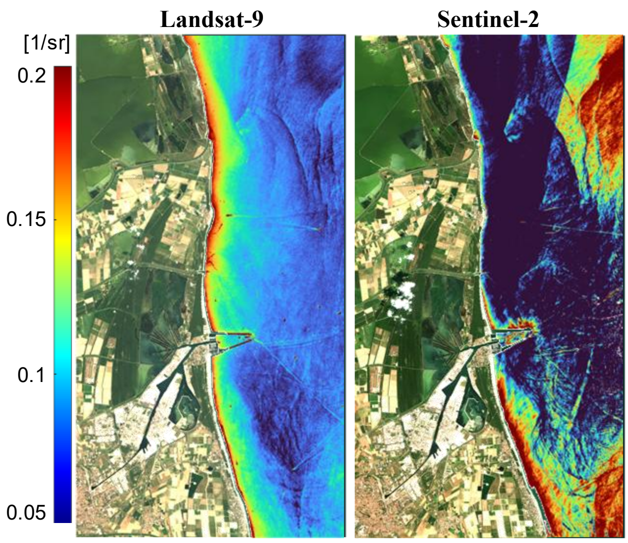

(a) 16 August 2023

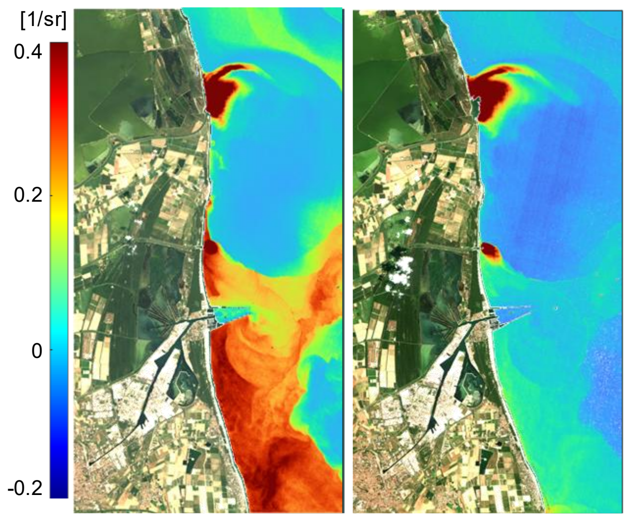

(b) 4 November 2023

Figure 3. Sun glint correction (g_{dd}) parameter retrieved from near-simultaneous Landsat-9 and Sentinel-2 images using WASI-AI.

As an example, for the August 2023 image, the averaged spectra of Landsat-9 and Sentinel-2 for the selected box (Figure 2a) in the northern part of the study area are compared before and after glint correction (Figure 4). The agreement between the two sensors improves markedly after correction, particularly in the blue–green region, where the spectral shapes become highly consistent. In addition, the reflectance in the long-wavelength (NIR) band centered near 865 nm becomes negligible for both sensors after glint correction, as the selected area shows deep and relatively clear waters.

Band [nm]	Before glint correction		After glint correction	
	R^2	NRMSD [%]	R^2	NRMSD [%]
443	0.83	11	0.90	6
482	0.79	9	0.87	5
561	0.85	13	0.91	8
655	0.82	14	0.86	9
865	0.83	12	0.89	8

Table 1. Consistency analysis of Landsat-9 and Sentinel-2 R_{rs} products before and after sun-glint correction

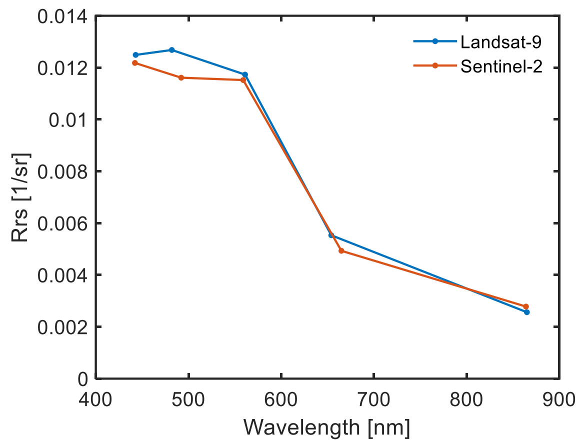

(a) before glint correction

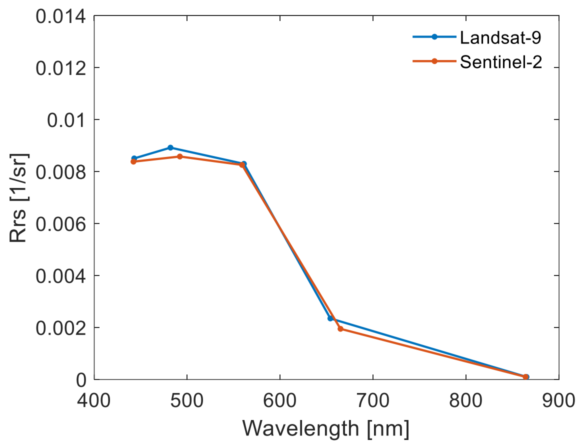

(b) after glint correction

Figure 4. Comparison of averaged Landsat-9 and Sentinel-2 spectra (a) before and (b) after glint correction for the selected box in the image acquired on 16 August 2023 (Figure 2a).

5. Conclusions and Future Work

The WASI-AI sun glint retrieval demonstrated that both the magnitude and spatial patterns of sun glint can vary significantly between images acquired only minutes apart. These variations arise from differences in sensor viewing geometry, sun zenith angle, as well as rapid changes in water surface roughness driven by currents and wind. The application of sun glint correction proved effective in enhancing the inter-sensor consistency of R_{rs}, which is particularly critical for the seamless retrieval of water constituents like Chl-a and TSM from multi-sensor imagery.

Although not the primary focus of this study, it is worth noting that Chl-a and TSM were also included among the fit parameters, and their retrievals likewise showed strong agreement between the two sensors after glint correction. As discussed earlier, estimating the g_{dd} parameter not only mitigates sun glint effects but also compensates for residual errors from the atmospheric-correction step. This combined mitigation enables the generation of consistent R_{rs} products from Landsat-9 and Sentinel-2 imagery.

Although the WASI-AI glint-correction approach was applied here to Landsat-9 and Sentinel-2 data, the method is inherently sensor-independent and can therefore be used with any multispectral or hyperspectral imagery. This flexibility facilitates multi-sensor analyses across a wide range of satellite and airborne platforms. While the improved multi-sensor consistency of the R_{rs} products after glint correction provides strong evidence of the method’s effectiveness, future work should include accuracy assessments using in-situ spectroradiometric measurements. It is important to note that the glint correction procedure in WASI-AI is performed simultaneously with the retrieval of other fit parameters (e.g., water constituent concentrations). Although this integrated approach offers clear advantages, it also requires full parameterization of all fit variables, which may be less straightforward when only glint-corrected R_{rs} is desired. In future studies, we aim to build a comprehensive dataset of g_{dd} products derived from WASI-AI inversions to support the development of deep-learning models capable of estimating sun-glint contributions independently of other fit parameters.

Acknowledgements

Adriatic coastal areas science-based solutions for climate adaptation (AdriaClimPlus-ITHR0200333) funded by the Interreg Italy-Croatia cooperation program.

References

Dörnhöfer, K., Göritz, A., Gege, P., Pflug, B., & Oppelt, N. (2016). Water Constituents and Water Depth Retrieval from Sentinel-2A—A First Evaluation in an Oligotrophic Lake. *Remote Sensing*, *8*(11), 941. https://doi.org/10.3390/rs8110941

Gege, P. (2012). Analytic model for the direct and diffuse components of downwelling spectral irradiance in water. *Applied Optics*, *51*(9), 1407–1419. https://doi.org/10.1364/AO.51.001407

Gege, P. (2014). WASI-2D: A software tool for regionally optimized analysis of imaging spectrometer data from deep and shallow waters. *Computers & Geosciences*, *62*, 208–215. https://doi.org/10.1016/J.CAGEO.2013.07.022

Gege, P., & Groetsch, P. (2016). A spectral model for correcting sun glint and sky glint. *Proc. Ocean Optics XXIII*.

Gordon, H. R. (1997). Atmospheric correction of ocean color imagery in the Earth Observing System era. *Journal of Geophysical Research: Atmospheres*, *102*(D14), 17081–17106. https://doi.org/https://doi.org/10.1029/96JD02443

Gregg, W. W., & Carder, K. L. (1990). A simple spectral solar irradiance model for cloudless maritime atmospheres. *Limnology and Oceanography*, *35*(8), 1657–1675. https://doi.org/10.4319/lo.1990.35.8.1657

Hafeez, S., Wong, M. S., Abbas, S., & Asim, M. (2022). Evaluating Landsat-8 and Sentinel-2 Data Consistency for High Spatiotemporal Inland and Coastal Water Quality Monitoring. *Remote Sensing*, *14*(13). https://doi.org/10.3390/rs14133155

Harmel, T., Chami, M., Tormos, T., Reynaud, N., & Danis, P. A. (2018). Sunglint correction of the Multi-Spectral Instrument (MSI)-SENTINEL-2 imagery over inland and sea waters from SWIR bands. *Remote Sensing of Environment*, *204*, 308–321. https://doi.org/10.1016/J.RSE.2017.10.022

Hochberg, E. J., Andrefouet, S., & Tyler, M. R. (2003). Sea surface correction of high spatial resolution Ikonos images to improve bottom mapping in near-shore environments. *IEEE Transactions on Geoscience and Remote Sensing*, *41*(7), 1724–1729. https://doi.org/10.1109/TGRS.2003.815408

Jerlov, N. G. (1976). *Marine Optics*. Elsevier Scientific Publ. Company.

Kay, S., Hedley, J. D., & Lavender, S. (2009). Sun Glint Correction of High and Low Spatial Resolution Images of Aquatic Scenes: a Review of Methods for Visible and Near-Infrared Wavelengths. *Remote Sensing*, *1*(4), 697–730. https://doi.org/10.3390/rs1040697

Khan, R. M., Salehi, B., Niroumand-Jadidi, M., & Mahdianpari, M. (2024). Mapping Water Clarity in Small Oligotrophic Lakes Using Sentinel-2 Imagery and Machine Learning Methods: A Case Study of Canandaigua Lake in Finger Lakes, New York. *IEEE Journal of Selected Topics in Applied Earth Observations and Remote Sensing*, *17*, 4674–4688. https://doi.org/10.1109/JSTARS.2024.3359648

Kutser, T., Vahtmäe, E., & Praks, J. (2009). A sun glint correction method for hyperspectral imagery containing areas with non-negligible water leaving NIR signal. *Remote Sensing of Environment*, *113*(10), 2267–2274. https://doi.org/https://doi.org/10.1016/j.rse.2009.06.016t

Lin, J., Miller, P. I., Jönsson, B. F., & Bedington, M. (2021). Early Warning of Harmful Algal Bloom Risk Using Satellite Ocean Color and Lagrangian Particle Trajectories. *Frontiers in Marine Science*, *Volume 8-2021*. https://doi.org/10.3389/fmars.2021.736262

Mobley, C. D. (1999). Estimation of the remote-sensing reflectance from above-surface measurements. *Applied Optics*, *38*(36), 7442. https://doi.org/10.1364/AO.38.007442

Ngamile, S., Madonsela, S., & Kganyago, M. (2025). Trends in remote sensing of water quality parameters in inland water bodies: a systematic review. *Frontiers in Environmental Science*, *Volume 13-2025*. https://doi.org/10.3389/fenvs.2025.1549301

Niroumand-Jadidi, M., & Bovolo, F. (2021). Water Quality Retrieval and Algal Bloom Detection Using High-Resolution Cubesat Imagery. *ISPRS Annals of the Photogrammetry, Remote Sensing and Spatial Information Sciences*, *V-3–2021*, 191–195. https://doi.org/10.5194/isprs-annals-V-3-2021-191-2021

Niroumand-Jadidi, M., & Bovolo, F. (2023). Deep-Learning-Based Retrieval of an Orange Band Sensitive to Cyanobacteria for Landsat-8/9 and Sentinel-2. *IEEE Journal of Selected Topics in Applied Earth Observations and Remote Sensing*, *16*, 3929–3937. https://doi.org/10.1109/JSTARS.2023.3266929

Niroumand-Jadidi, M., Bovolo, F., Bresciani, M., Gege, P., & Giardino, C. (2022). Water Quality Retrieval from Landsat-9 (OLI-2) Imagery and Comparison to Sentinel-2. *Remote Sensing*, *14*(18). https://doi.org/10.3390/rs14184596

Niroumand-Jadidi, M., Bovolo, F., Bruzzone, L., & Gege, P. (2020). Physics-based Bathymetry and Water Quality Retrieval Using PlanetScope Imagery: Impacts of 2020 COVID-19 Lockdown and 2019 Extreme Flood in the Venice Lagoon. *Remote Sensing 2020, Vol. 12, Page 2381*, *12*(15), 2381. https://doi.org/10.3390/RS12152381

Niroumand-Jadidi, M., Bovolo, F., Bruzzone, L., & Gege, P. (2021). Inter-Comparison of Methods for Chlorophyll-a Retrieval: Sentinel-2 Time-Series Analysis in Italian Lakes. *Remote Sensing*, *13*(12), 2381. https://doi.org/10.3390/rs13122381

Niroumand-Jadidi, M., & Gege, P. (2025). WASI-AI: Synergistic Integration of AI and Physics for Retrieving Water Quality and Benthic Parameters from Multi- and Hyperspectral Images. *IEEE Journal of Selected Topics in Applied Earth Observations and Remote Sensing*, *18*, 22832–22846. https://doi.org/10.1109/JSTARS.2025.3605061

Niroumand-Jadidi, M., Legleiter, C. J., & Bovolo, F. (2025). Neural Network-Based Temporal Ensembling of Water Depth Estimates Derived from SuperDove Images. *Remote Sensing*, *17*(7). https://doi.org/10.3390/rs17071309

Toming, K., Kutser, T., Laas, A., Sepp, M., Paavel, B., & Nõges, T. (2016). First Experiences in Mapping Lake Water Quality Parameters with Sentinel-2 MSI Imagery. *Remote Sensing*, *8*(8), 640. https://doi.org/10.3390/rs8080640

Vanhellemont, Q. (2019). Adaptation of the dark spectrum fitting atmospheric correction for aquatic applications of the Landsat and Sentinel-2 archives. *Remote Sensing of Environment*, *225*, 175–192. https://doi.org/https://doi.org/10.1016/j.rse.2019.03.010

Vanhellemont, Q., & Ruddick, K. (2018). Atmospheric correction of metre-scale optical satellite data for inland and coastal water applications. *Remote Sensing of Environment*, *216*, 586–597. https://doi.org/https://doi.org/10.1016/j.rse.2018.07.015

Zaghian, S., Mohammadzadeh, A., Ghorbanian, A., Bovolo, F., & Niroumand-Jadidi, M. (2023). Enhancing suspended sediment concentration retrieval by integrating thermal infrared and optical bands of Landsat-8 and machine learning algorithms. *International Journal of Remote Sensing*, *44*(18), 5814–5844. https://doi.org/10.1080/01431161.2023.2255350